

Article

Hydroelastic Waves in a Frozen Channel with Non-Uniform Thickness of Ice

Konstantin Shishmarev ^{1,*}, Kristina Zavyalova ¹, Evgeniy Batyaev ² and Tatyana Khabakhpasheva ²

¹ Department of Differential Equations, Altai State University, 656049 Barnaul, Russia; kristina-zavyalova-1996@mail.ru

² Lavrentyev Institute of Hydrodynamics SB RAS, 630090 Novosibirsk, Russia; john@hydro.nsc.ru (E.B.); tkhab@ngs.ru (T.K.)

* Correspondence: shishmarev.k@mail.ru

Abstract: The periodic flexural-gravity waves propagating along a frozen channel are investigated. The channel has a rectangular cross section. The fluid in the channel is inviscid, incompressible and covered with ice. The ice is modeled by a thin elastic plate whose thickness varies linearly. Two cases have been considered: the ice thickness varies symmetrically across the channel, being the smallest at the center of the channel and the largest at the channel walls; the ice thickness varies from the smallest value at the one wall to the largest value at another wall. The periodic 2D problem is reduced to the problem of the wave profiles across the channel. The solution of the last problem is obtained by the normal mode method of an elastic beam with linear thickness. The behavior of flexural-gravity waves depending on the inclination parameter of the ice thickness has been studied and the results have been compared with those for a constant-thickness plate. Dispersion relations, profiles of flexural-gravity waves across the channel and distributions of strain in the ice cover have been determined. In the asymmetric case, it is shown that for long waves, the most probable plate failure corresponds to transverse strains at the thin edge of the plate, which can lead to detachment of the ice from the corresponding bank. For short waves, the longitudinal stresses within the plate, localized closer to the thick edge, become maximum. This can lead to cracking of the plate in transverse direction. In the symmetric case, the maximum strains are achieved inside the plate—close to the center, but not necessarily in the midpoint.

Keywords: flexural-gravity waves; channel; ice cover; non-uniform thickness of ice; elastic plate; dispersion relations; critical speed



Citation: Shishmarev, K.; Zavyalova, K.; Batyaev, E.; Khabakhpasheva, T. Hydroelastic Waves in a Frozen Channel with Non-Uniform Thickness of Ice. *Water* **2022**, *14*, 281. <https://doi.org/10.3390/w14030281>

Academic Editors: Yury Stepanyants, Trilochan Sahoo and Mike Meylan

Received: 5 December 2021

Accepted: 13 January 2022

Published: 18 January 2022

Publisher's Note: MDPI stays neutral with regard to jurisdictional claims in published maps and institutional affiliations.



Copyright: © 2022 by the authors. Licensee MDPI, Basel, Switzerland. This article is an open access article distributed under the terms and conditions of the Creative Commons Attribution (CC BY) license (<https://creativecommons.org/licenses/by/4.0/>).

1. Introduction

The problem of flexural-gravity wave propagation in the ice covers has been actively investigated for the last decades in the context of the development of Polar territories and the possibility of long-term use of the Northern Sea Route. These studies have also become particularly relevant in connection with the discovery and development of natural oil and gas reserves in the Arctic and, possibly, Antarctic shelf. The main part of the flexural-gravity wave research was carried out for ice sheets of infinite extent. However, majority of the ice tanks, where scientific and technical experiments with ice cover are conducted, have finite dimensions and rectangular cross-sections. For this reason, studying the features of waves in channels and how they differ from waves in unbounded sheets is highly important. In addition, channels can also be considered as a simple model of rivers in northern countries, where they are frozen in winter time and can be used for transportation giving access to remote areas. Maintaining the integrity of the ice cover is an important issue when moving cargo and people on ice. In this context, there are many problems related to conditions of ice cover preservation and/or destruction, including those caused by propagating waves and moving load. The boundary conditions on the channel walls significantly affect the results of these studies.

One of the first consideration of flexural-gravity waves was done by Greenhill in [1]. Models of waves in ice cover were further developed by Kheysin [2] where ice was modeled by a linear elastic plate. Reviews of works on hydroelastic waves in unbounded regions can be found in [2–6]. The model of linear elastic plate is still the main one, although viscoelastic and poroelastic models of the ice cover are also considered by many authors [7–12]. Nonlinear models, models that take into account ice compression and the presence of cracks in ice sheets, also have been actively developed [13–23].

The presence of walls and particular conditions on them change the mathematical formulation of the problem and, consequently, the properties of the solution [24,25]. It was shown in [5,26] that for waves in the ice channel with rectangular cross-section, there is an infinite number of hydroelastic waves with the same length and different forms across the channel propagating along the channel. In this case, each waveform has its own dispersion relation and critical velocity of propagation. The significance of critical speeds is clearly demonstrated in the problems of load motion along the ice cover.

In the framework of the linear theory of elastic plates, if a load moves at the critical speed, the deflection of the floating ice plate and the stresses in it increase beyond all bounds. In reality, they are limited by dissipation or non-linearity, which linear models do not take into account. In order to break the ice sheet by a moving load, such as hovercraft or submarine, this load must move along the ice sheet at a certain speed, which is close to the critical speed. Then, the stresses in the ice plate will be large enough to break the ice. This method of ice destruction was called “resonant method of ice-breaking” and was mentioned the first time in [27], among several patents for the ice destruction by hovercraft. The resonant method was studied theoretically, numerically and experimentally by Kozin and his group [28–31]. Experimental results on effective hovercraft motion was provided in [32] with data being obtained in the ice tank at the Institute for Marine Dynamics (IMD) in Newfoundland. It was shown that air-cushion vehicles can be effective icebreakers. Investigations of critical speeds for loads moving along ice channels was performed in [10,33,34]. It was shown that if the load moves at a speed lower than the first critical speed, the ice plate deflection is formed in the vicinity of the load, and if the load moves at a supercritical speed, a system of hydroelastic waves propagating from the load is formed. The number of waves in this system is finite and depends on the relation of the load velocity to the critical velocities for flexural-gravity waves in the channel. Effect of ice cracks on ice destruction by a load moving with resonant speed was investigated in [35]. The possibility of ice destruction by turbulent fluctuations of atmospheric pressure in wind conditions was studied. It was shown that an ice sheet with initial cracks can be destructed more easily than a continuous one due to the possible growth of cracks.

However, under natural conditions, the ice cover is not homogeneous. Due to different reasons, its thickness, density and stiffness are not constant. This paper considers the case of an ice cover whose thickness varies linearly, and ice density and stiffness are assumed to be constant. The problem is solved by the method of normal modes, see [5,26]. The normal modes describe free oscillations of a dry elastic plate with appropriate boundary conditions. Within this method, the problem reduces to a system of algebraic equations with pre-calculated coefficients. Therefore, analytical formulae for normal modes of the plate with linearly varying thickness will be an advantage of this method and is important for successful solution of the problem.

Vibrations of the plate with varying thickness and beam with varying cross-sections have been studied in engineering problems of narrow high-rise buildings. In [36], it is written: “In fact, there are very few equations of vibrating plates with variable cross-section where exact solutions can be obtained. These exact plate solutions are available only for certain plate shapes and boundary conditions (e.g., Timoshenko and Woinowsky-Krieger, 1959)”. The vibrations of a beam of linear rigidity in longitudinal direction were studied in the book by Timoshenko [37] by approximate methods through the representation of the solution in the form of a power series on the parameter of cross-section variation. The coefficients of this series are functions of the longitudinal coordinate. They are determined

from a system of differential equations. These functions are sought in the form of series using the method of separation of variables. The vibration characteristics of stepped thickness plates of rectangular shape with simply supported edges were investigated in [38].

The equations of static equilibrium of shear and flexural vibrations of a beam with linearly or polynomially varying thickness $(h + x)^n$ along the beam were presented in [39] in the form of a self-adjoint differential equation of second-order, here h is a minimum value of a beam thickness and x is a coordinate along a beam. It has been shown in [36] that for this varying thickness and rigidity of a beam behaving as $(h + x)^{3n}$, equations of vibrating plates can be reduced to Bessel’s equations or Euler’s equation. The general solutions were derived in the form of Bessel’s and modified Bessel’s functions. Similar functions for the investigation of free vibrations of plates with linearly varying thickness were used in [40]. In [41], these functions are defined by using the shoot method.

Vibrations of plates with variable thickness were also studied in [42], where orthogonality of the modes with the weight equal to the plate thickness was proved. This orthogonality property of the normal modes is used in the present paper.

In this paper, we shall study a problem of hydroelastic waves propagating along a frozen channel with linearly varying ice thickness within two cases of the variation: symmetric and asymmetric. The main attention is given to the effect of variable thickness on characteristics of periodic waves. The formulation of the problem is given in Section 2. The method of the solution is presented in Section 3. The problem using the described methods is reduced to an eigenvalue and eigenvector problem in matrix form which we solved numerically. The analysis of the numerical results is carried out for parameters of the problem modeling an experimental ice tank at the Sholem Aleichem Amur State University in Birobidzhan (see [31]). The results of the analysis are discussed in Section 4. Dispersion relations, phase and group speeds, profiles of the waves across the channel, maximum strains in the ice cover and their directions are studied.

2. Formulation of the Problem

Periodic hydroelastic waves propagating along a frozen channel are considered. The channel is of rectangular section with a finite depth H ($-H < z < 0$) and a finite width $2b$ ($-b < y < b$), the channel is of infinite extent in the x direction. Here, $Oxyz$ is a Cartesian coordinate system. The scheme of the channel is shown in Figure 1a. Liquid in the channel is inviscid, incompressible and covered with ice. Flow beneath the plate is potential. The ice is modeled by a thin elastic plate with given constant density ρ_i and rigidity $D(y)$, where $D(y) = Eh_i^3(y) / [12(1 - \mu^2)]$, E is the Young’s modulus for ice, μ is the Poisson ratio for ice and $h_i(y)$ is the non-uniform thickness of the ice cover. We are concerned with the linear change in the ice thickness across the channel. The function $h_i(y)$ will be specified later. The ice thickness is constant along the channel.

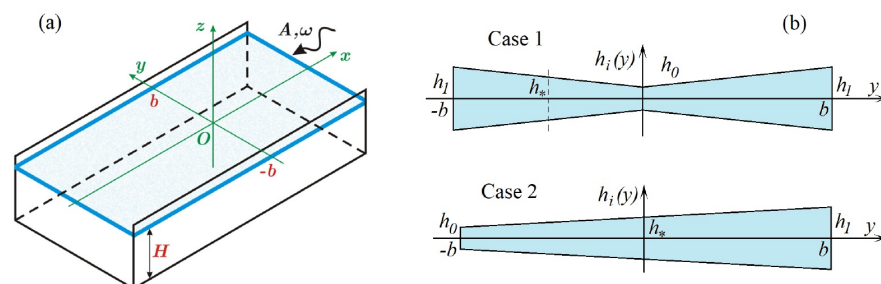


Figure 1. Scheme of the channel (a). Schemes of the profile of the ice across the channel (b).

The problem is studied within the linear theory of hydroelasticity. Deflections of the ice plate are governed by the Kirchhoff–Love theory (see, e.g., [37]). The basic assumption of this theory is that the plate is thin, and then, deflections of the plate are described by

the vertical displacement of the midsurface of the plate $z = w(x, y, t)$. It is also assumed that the ice deflections are much smaller than all linear dimensions in the plate plane. In the case of periodic hydroelastic waves propagating along the channel, it is expected that the ice deflections $w(x, y, t)$ caused by these waves have small amplitude compared to the wavelength and width of the channel $2b$. Another condition is that the wave frequencies must be low so that the linearized Bernoulli equation can be used.

The mathematical formulation of the problem consists of two coupled parts. The first part is related to the determination of ice deflections (vertical displacement of a plate from a state of rest, $z = 0$). The ice deflection $w(x, y, t)$ satisfies the equation of a thin elastic plate

$$\frac{\partial Q_x}{\partial x} + \frac{\partial Q_y}{\partial y} - h_i(y)\rho_i \frac{\partial^2 w}{\partial t^2} + p(x, y, 0, t) = 0 \quad (-\infty < x < \infty, -b < y < b, z = 0). \quad (1)$$

$$Q_x = \frac{\partial M_x}{\partial x} + \frac{\partial M_{xy}}{\partial y}, \quad Q_y = \frac{\partial M_{yx}}{\partial x} + \frac{\partial M_y}{\partial y}. \quad (2)$$

Functions $Q_x(x, y)$ and $Q_y(x, y)$ are transverse shears. Corresponding bending $M_x(x, y)$, $M_y(x, y)$ and twisting moments M_{xy} caused by elastic forces are

$$M_x = -D \left(\frac{\partial^2 w}{\partial x^2} + \mu \frac{\partial^2 w}{\partial y^2} \right), \quad M_y = -D \left(\frac{\partial^2 w}{\partial y^2} + \mu \frac{\partial^2 w}{\partial x^2} \right), \quad M_{xy} = -(1 - \mu)D \frac{\partial^2 w}{\partial x \partial y}. \quad (3)$$

Here, $p(x, y, 0, t)$ —liquid pressure at the ice/liquid interface—is determined through the linearized Bernoulli integral

$$\frac{p(x, y, 0, t)}{\rho_\ell} = -\frac{\partial \varphi}{\partial t}(x, y, 0, t) - gw, \quad (4)$$

where ρ_ℓ —density of the liquid, g —acceleration of gravity and $\varphi(x, y, z, t)$ —flow potential in the channel. The ice plate is frozen to the channel walls. This is modeled by the clamped conditions of ice deflection at the walls

$$w = 0, \quad w_y = 0, \quad (y = \pm b). \quad (5)$$

The second part of the problem is related to the description of the hydrodynamics in the channel. The potential $\varphi(x, y, z, t)$ satisfies the Laplace equation in the channel domain

$$\frac{\partial^2 \varphi}{\partial x^2} + \frac{\partial^2 \varphi}{\partial y^2} + \frac{\partial^2 \varphi}{\partial z^2} = 0 \quad (-\infty < x < \infty, -b < y < b, -H < z < 0), \quad (6)$$

boundary conditions of impermeability at rigid boundaries of the channel (walls and bottom) and linearized kinematic condition at the ice/liquid interface

$$\frac{\partial \varphi}{\partial y} = 0 \quad (y = \pm b), \quad \frac{\partial \varphi}{\partial z} = 0 \quad (z = -H), \quad \frac{\partial \varphi}{\partial z} = \frac{\partial w}{\partial t} \quad (z = 0). \quad (7)$$

To justify the linearization of the interface condition, let us write out the original nonlinear condition

$$\nabla \varphi \cdot \vec{n} = \vec{V}_b \cdot \vec{n},$$

where V_b is the body velocity, $V_b = (0, 0, w_t)$. This condition is satisfied at the lower surface of the plate $z = w(x, y, t) - h_i(y)/2$ with corresponding normal vector and can be written in the form

$$\frac{\partial \varphi}{\partial z} = \frac{\partial w}{\partial t} + \frac{\partial w}{\partial x} \frac{\partial \varphi}{\partial x} + \left(\frac{\partial w}{\partial y} - \frac{1}{2} \frac{dh'_i}{dy} \right) \frac{\partial \varphi}{\partial y}.$$

All derivatives $\varphi_x, \varphi_y, \varphi_z, w_x, w_y, w_t$ in this equation are small with the same order. So, the second and third term on the RHS of this equation can be neglected as second-

order terms. We can neglect the term with $h'_i(y)$ and use the linearized condition (7) if this derivative is small with the same order, but we can state in advance that for the cases of linear change of plate thickness considered in this paper (see Figure 1b), $h'_i(y) < h_*/b$ and we should assume $h_i(y) \ll b$. How small $h'_i(y)$ is in our calculations will be discussed in Section 4.

Unknown functions w and φ are sought in the form of periodic hydroelastic waves propagating along the channel with constant amplitude A , wavenumber k and frequency ω

$$w(x, y, t) = ARe(F(y)e^{i(kx+\omega t)}), \tag{8}$$

$$\varphi(x, y, t) = ARe(i\Phi(y, z)e^{i(kx+\omega t)}). \tag{9}$$

Using this form, we shall determine the dispersion relations $\omega(k)$ and other characteristics of the periodic waves. The main focus of the study is on the effect of the non-uniform ice thickness $h_i(y)$ on the listed parameters.

Two cases of linear change in the ice thickness are considered (Figure 1b). The first case is a case of a symmetric change in the ice thickness with the smallest value at the center line of the channel and the largest at the walls of the channel. The second case is a case of an asymmetric change in the ice thickness with the smallest value at one of the walls (in the considered case at the left edge of the plate) and the largest value at the opposite wall. Further, we will refer to these cases as Case 1 (symmetric) and Case 2 (asymmetric), respectively. The thickness of the ice is a function of the transverse coordinate y . The main parameters of the thickness are its average h_* , minimum h_0 and maximum h_1 values (see Figure 1b). Then, $h_i(y)$ can be written in the form:

Case 1

$$h_i(y) = h_0(1 + \alpha_1|y/b|), \quad \alpha_1 = \frac{h_1 - h_0}{h_0}, \quad h_i(0) = h_0, \quad h_i(\pm b) = h_1. \tag{10}$$

Case 2

$$h_i(y) = h_*(1 + \alpha_2 y/b), \quad \alpha_2 = \frac{h_1 - h_0}{h_1 + h_0}, \quad h_i(-b) = h_0, \quad h_i(b) = h_1. \tag{11}$$

The results of the problem will be compared with each other in both cases for the same values of h_0, h_* and h_1 . Note that for the same values of these parameters, $\alpha_1 \neq \alpha_2$.

The problem (1)–(9) is solved in dimensionless variables. Further, all variables and functions are written in dimensionless form and have the same notations as the dimensional ones. Length scale is taken to be half the channel width b , the time scale is $1/\omega$, the amplitude A is the scale of the ice deflection, $\rho_\ell g A$ is the scale of the liquid pressure, $Ab\omega$ is the scale of the flow velocity potential. The scale h_{sc} of the function $h_i(y)$ is chosen depending on the case: in Case 1— h_0 , in Case 2— h_* . Note that the scales of the ice deflection and the flow velocity potential are proportional to the amplitude A due to the linearity of the problem, and the parameter A can be arbitrary. In dimensionless variables, the channel cross-sectional boundaries are: $(-1 < y < 1), (-h < z < 0)$, where $h = H/b$ is the dimensionless channel depth. The functions of the profiles of the ice deflection and the velocity potential $F(y)$ and $\Phi(y, z)$ are dimensionless. The functions $F(y)$ are determined up to the amplitude; therefore, a normalization condition should be imposed on them. In general, the dimensionless wavenumber $\kappa, \kappa = kb$, and the profile function $F(y)$ can be complex. However, these solutions correspond to waves whose amplitude increases as $x \rightarrow +\infty$ or $x \rightarrow -\infty$. Therefore, we will consider only solutions with positive and real k and real $F(y)$. Note that in the considered formulation, there are no initial conditions and boundary conditions for $|x| \rightarrow \infty$.

A similar problem for an ice plate of constant thickness was studied in [5]. In this paper, we restrict ourselves to solving the problem with the clamped conditions at the channel walls (5). Other boundary conditions can be investigated by a similar method, as

it was done, for example, for a plate of constant thickness and free boundary conditions in [5].

In the dimensionless variables equation of the plate, Equation (1) reads

$$\beta \left[h_i^3(y) \left(\frac{\partial^4 w}{\partial x^4} + 2 \frac{\partial^4 w}{\partial x^2 \partial y^2} + \frac{\partial^4 w}{\partial y^4} \right) + 6h_i^2(y) \frac{dh_i}{dy} \left(\frac{\partial^3 w}{\partial x^2 \partial y} + \frac{\partial^3 w}{\partial y^3} \right) + 6h_i(y) \left(\frac{dh_i}{dy} \right)^2 \left(\frac{\partial^2 w}{\partial y^2} + \mu \frac{\partial^2 w}{\partial x^2} \right) \right] + \delta \gamma \frac{\partial^2 w}{\partial t^2} = p(x, y, 0, t), \tag{12}$$

where $\beta = D_* / [\rho_\ell g b^4]$, $D_* = E h_{sc}^3 / [12(1 - \mu^2)]$, $\gamma = b \omega^2 / g$ and $\delta = h_{sc} \rho_i / [b \rho_\ell]$. The problem (1)–(9) is rewritten in terms of $F(y)$ and $\Phi(y, z)$. Substituting (8) and (9) into (12) gives

$$\beta \left[h_i^3(y) (\kappa^4 F - 2\kappa^2 F'' + F'''') + 6h_i^2(y) h_i' (-\kappa^2 F' + F''') + 6h_i(y) (h_i')^2 (F'' - \mu \kappa^2 F) - \frac{\delta \gamma}{\beta} F \right] = \gamma \Phi(y, 0) - F, \tag{13}$$

where prime stands for the derivative with respect to y . Note that $h_i' = \text{sign}(y) \cdot \alpha_1$ in Case 1 and $h_i' = \alpha_2$ in Case 2. The rest of the equations of the problem in the dimensionless variables are

$$F = 0, \quad F_y = 0 \quad (y = \pm 1), \tag{14}$$

$$\Phi_{yy} + \Phi_{zz} = \kappa^2 \Phi \quad (-1 < y < 1, -h < z < 0), \tag{15}$$

$$\Phi_y = 0 \quad (y = \pm 1), \quad \Phi_z = 0 \quad (z = -h), \quad \Phi_z = F \quad (z = 0). \tag{16}$$

The solution of the problem (13)–(16) depends on the three dimensionless parameters β , γ and δ . We shall find dispersion relations $\omega(k)$ for some typical values of parameters of the problem. The values of these parameters correspond to the parameters of the experimental ice tank at the Sholem Aleichem Amur State University in Birobidzhan [31]. The only difference is the non-uniform ice thickness, the effect of which will be investigated. In further calculations, the average ice thickness h_* is usually equal to the declared constant ice thickness in the ice tank.

All presented results are valid for the real parameters with conditions $A \ll 2b$, $A \ll \lambda$ and $h_i \ll 2b$, where λ is a wavelength of the propagating wave and the dimensionless ice deflection w is of order 1. In addition, the square of the slope of ice deflections must be negligible. If one wants to apply the results of this article to plates with large plate thickness, one needs to take into account these conditions. For example, for the plate of 1 m thickness, the ice deflections comparable with the plate thickness should be caused by hydroelastic waves with their wavelength greater than 10 m and the considered area of the plate must be also greater than 10 m in both plane directions. Moreover, one needs to be careful with possible large values of $h_i'(y)$ which can occur in a plate with large thickness because, in this case, the kinematic condition for vertical displacement of the plate in the form $w_t = \varphi_z$ cannot be used.

3. Method of the Solution

Rearranging terms in Equation (13), one can notice a combination of terms in the form

$$h_i(y) [h_i^2(y) F'''' + 6h_i(y) h_i' F'''] + 6(h_i')^2 F'']. \tag{17}$$

The part in square brackets in (17) gives the LHS of the Bessel differential equation in the considered case of linear change in thickness $h_i(y)$. Therefore, it is convenient to seek the solution of Equation (13) in the form of the infinite series

$$F(y) = \sum_{n=1}^{\infty} a_n \psi_n(y), \tag{18}$$

where a_n are principal coordinates and $\psi_n(y)$ are the solutions of the spectral problem

$$h_i^2(y)\psi_n'''' + 6h_i(y)h_i'\psi_n'''' + 6(h_i')^2\psi_n'' = \theta_n^4\psi_n \quad (-1 < y < 1), \tag{19}$$

$$\psi_n = 0, \quad \psi_n' = 0 \quad (y = \pm 1), \tag{20}$$

where θ_n are the eigenvalues of the problem (19)–(20). This spectral problem is obtained from the problem of natural frequencies and clamped modes of an elastic beam with linear thickness (see, e.g. [36]). It can be shown (see [36,40]) that the non-trivial solution of Equation (19) is

$$\psi_n(y) = \frac{1}{\xi} [A_n J_1(\eta_n \xi) + B_n Y_1(\eta_n \xi) + C_n I_1(\eta_n \xi) + D_n K_1(\eta_n \xi)], \quad n = 1, 2, 3, \dots \tag{21}$$

where $\eta_n = 2\theta_n/\alpha$, $\xi = \sqrt{1 + \alpha y}$ (α is equal to α_1 or α_2 depending on the case) and J, Y, I, K are Bessel functions. Parameters A_n, B_n, C_n and D_n are determined from the boundary conditions and the normalization condition for the functions ψ_n . The modes $\psi_n(y)$ will be determined for Case 1 and Case 2, separately. These functions for a beam with constant thickness are well known, see, e.g., [5].

Case 1. In this case, Equation (19) is separated and $\psi_n(y)$ satisfies one of the two equations depending on the sign of y

$$(1 + \alpha_1 y)^2 \psi_n'''' + 6\alpha_1(1 + \alpha_1 y)\psi_n'''' + 6\alpha_1^2 \psi_n'' = \theta_n^4 \psi_n \quad (0 \leq y < 1), \tag{22}$$

$$(1 - \alpha_1 y)^2 \psi_n'''' - 6\alpha_1(1 - \alpha_1 y)\psi_n'''' + 6\alpha_1^2 \psi_n'' = \theta_n^4 \psi_n \quad (-1 < y < 0). \tag{23}$$

It is easy to show that both even and odd functions can be a solution of system of Equations (22)–(23). These solutions will be found independently of each other using the same algorithm. First, we find a solution of Equation (22), then, in the even or odd way, depending on the case, we continue the found solution to negative values of y . For both solutions, the boundary conditions at $y = 1$ are the same, but at $y = 0$, they are different.

Odd modes $\psi_n(y)$ are solutions of spectral problem with governing Equation (22), boundary conditions at ($y = 1$)

$$A_n J_1(\eta_n \xi_+) + B_n Y_1(\eta_n \xi_+) + C_n I_1(\eta_n \xi_+) + D_n K_1(\eta_n \xi_+) = 0, \tag{24}$$

$$A_n J_0(\eta_n \xi_+) + B_n Y_0(\eta_n \xi_+) + C_n I_0(\eta_n \xi_+) - D_n K_0(\eta_n \xi_+) = 0, \tag{25}$$

where $\xi_+ = \sqrt{1 + \alpha_1}$ and boundary conditions of zero ice deflections and zero bending moment at the center of the beam, ($y = 0$)

$$A_n J_1(\eta_n \xi_0) + B_n Y_1(\eta_n \xi_0) + C_n I_1(\eta_n \xi_0) + D_n K_1(\eta_n \xi_0) = 0, \tag{26}$$

$$A_n J_0(\eta_n \xi_0) + B_n Y_0(\eta_n \xi_0) + C_n I_0(\eta_n \xi_0) - D_n K_0(\eta_n \xi_0) - \eta_n \psi_{1n}(\xi_0) = 0, \tag{27}$$

$$\psi_{1n}(\xi_0) = -A_n J_1(\eta_n \xi_0) - B_n Y_1(\eta_n \xi_0) + C_n I_1(\eta_n \xi_0) + D_n K_1(\eta_n \xi_0).$$

Here, $\xi_0 = 1$. Even modes $\psi_n(y)$ are the solutions of the same spectral problem with conditions (26)–(27) replaced by conditions of zero slope and zero transverse shears of a beam with non-uniform thickness at its center

$$A_n J_1(\eta_n \xi_0) + B_n Y_1(\eta_n \xi_0) + C_n I_1(\eta_n \xi_0) + D_n K_1(\eta_n \xi_0) - \eta_n \psi_{0n}(\xi_0)/2 = 0, \tag{28}$$

$$\psi_{1n}(\xi_0) - \eta_n \psi_{2n}(\xi_0)/2 = 0, \tag{29}$$

$$\psi_{0n}(\xi_0) = A_n J_0(\eta_n \xi_0) + B_n Y_0(\eta_n \xi_0) + C_n I_0(\eta_n \xi_0) - D_n K_0(\eta_n \xi_0),$$

$$\psi_{2n}(\xi_0) = -A_n J_0(\eta_n \xi_0) - B_n Y_0(\eta_n \xi_0) + C_n I_0(\eta_n \xi_0) - D_n K_0(\eta_n \xi_0).$$

Case 2. Modes $\psi_n(y)$ are the solutions of the spectral problem

$$(1 + \alpha_2 y)^2 \psi_n'''' + 6\alpha_2(1 + \alpha_2 y) \psi_n'''' + 6\alpha_2^2 \psi_n'' = \theta_n^4 \psi_n \quad (-1 < y < 1), \tag{30}$$

with boundary conditions (20) in the form

$$A_n J_1(\eta_n \xi_{\pm}) + B_n Y_1(\eta_n \xi_{\pm}) + C_n I_1(\eta_n \xi_{\pm}) + D_n K_1(\eta_n \xi_{\pm}) = 0, \tag{31}$$

$$A_n J_0(\eta_n \xi_{\pm}) + B_n Y_0(\eta_n \xi_{\pm}) + C_n I_0(\eta_n \xi_{\pm}) - D_n K_0(\eta_n \xi_{\pm}) = 0, \tag{32}$$

where $\xi_{\pm} = \sqrt{1 \pm \alpha_2}$. Note that there are no even or odd solutions in Case 2.

The system of the equations for A_n, B_n, C_n and D_n (for example, Equations (31)–(32) in Case 2), can be written in a matrix form with the matrix denoted by A for both cases. The eigenvalues η_n are the solutions of the equation $\det(A) = 0$. Parameters A_n, B_n, C_n and D_n are the coordinates of the corresponding eigenvectors. There will be infinitely many solutions of this system.

The functions $\psi_n(y)$ are orthogonal with respect to a weighted inner product, where the weight function is equal to $h_i(y)$

$$\int_{-1}^1 (1 + \alpha y) \psi_n(y) \psi_m(y) dy = 0 \quad (n \neq m) \tag{33}$$

and A_n, B_n, C_n, D_n are normalized in such a way that the integral in (33) is equal to 1 for $n = m$. The orthogonality condition (33) is correct in both cases, if the weight $(1 + \alpha y)$ is replaced by $(1 + \alpha_1 |y|)$ in Case 1 or by $(1 + \alpha_2 y)$ in Case 2. In Case 1, this orthogonality can be considered on the segment $[0, 1]$. It is easy to show that for both even and odd solutions, in Case 1, the following condition holds

$$\int_0^1 (1 + \alpha_1 y) \psi_n(y) \psi_m(y) dy = 0 \quad (n \neq m).$$

To check this condition, one should use the boundary conditions for ψ_n at $y = 0$. When $n = m$, the last integral product is normalized by $1/2$.

The modes $\psi_n(y)$ depend on $\alpha_{1,2}$. One can estimate that $\psi_n(y)$ tend to normal modes of the thin elastic beam with constant thickness h_* when $\alpha \rightarrow 0$. The calculations show that dispersion relations for both cases of the non-uniform beam approximate dispersion relations of the beam with constant thickness, $h_i = 0.0035$ m, with visual accuracy for $h_* = 0.0035$ m, $h_0 = 0.00345$ m and $h_1 = 0.00355$ m in both cases. These values correspond to $\alpha_2 \approx 0.028$ and $\alpha_1 \approx 0.014$.

The kinematic condition (16) shows that the profile $\Phi(y, z)$ of the flow potential in the cross-section of the channel can be sought in the form

$$\Phi(y, z) = \sum_{n=1}^{\infty} a_n \Phi_n(y, z) \tag{34}$$

and Φ_n are the solutions of the boundary value problems

$$\frac{\partial^2 \Phi_n}{\partial y^2} + \frac{\partial^2 \Phi_n}{\partial z^2} = \kappa^2 \Phi_n, \tag{35}$$

$$\frac{\partial \Phi_n}{\partial y} = 0 \quad (y = \pm 1), \quad \frac{\partial \Phi_n}{\partial z} = 0 \quad (z = -h), \quad \frac{\partial \Phi_n}{\partial z} = \psi_n \quad (z = 0).$$

It can be shown that

$$\Phi_n(y, z) = \frac{1}{2} \Phi_{n0}^c(z) + \sum_{k=1}^{\infty} \Phi_{nk}^c(z) \cos(\pi ky) + \sum_{l=1}^{\infty} \Phi_{nl}^s(z) \sin[(\pi l - \pi/2)y],$$

where

$$\begin{aligned} \Phi_{nk}^c &= \frac{\psi_{nk}^c \cosh \mu_k^c(z+h)}{\mu_k^c \sinh \mu_k^c h}, & \Phi_{nl}^s &= \frac{\psi_{nl}^s \cosh \mu_l^s(z+h)}{\mu_l^s \sinh \mu_l^s h}, \\ \psi_{nk}^c &= \int_{-1}^1 \psi_n(y) \cos(\pi ky) dy, & \psi_{nl}^s &= \int_{-1}^1 \psi_n(y) \sin[(\pi l - \pi/2)y] dy, \\ \mu_k^c &= \sqrt{\kappa^2 + (\pi k)^2} & \mu_l^s &= \sqrt{\kappa^2 + (\pi l - \pi/2)^2}. \end{aligned}$$

In Case 1, only one type of coefficient should be considered, Φ_{nk}^c or Φ_{nk}^s , depending on the even or odd solution, respectively. In Case 2, both series of coefficients should be taken into account.

For each of the two cases, its own pair of functions F and Φ are determined. Substituting (17) and (34) into Equation (13), we arrive at the infinite system of equations to find the principal coordinates a_n

$$\begin{aligned} &\sum_{n=1}^{\infty} a_n \left\{ \beta(1 + \alpha_1|y|) \theta_n^4 \psi_n + \kappa^4 \beta(1 + \alpha_1|y|)^3 \psi_n \right. \\ &\quad \left. - 2\kappa^2 \beta \left((1 + \alpha_1|y|)^3 \psi_n'' + 3\alpha_1 \cdot \text{sign}(y) (1 + \alpha_1|y|)^2 \psi_n' \right) \right. \\ &\quad \left. - \kappa^2 6\alpha_1^2 \mu \beta(1 + \alpha_1|y|) \psi_n - \delta \gamma (1 + \alpha_1|y|) \psi_n - \gamma \Phi_n(y, 0) + \psi_n \right\} = 0. \end{aligned} \tag{36}$$

The last equation is written for Case 1. For Case 2, one needs to replace α_1 with α_2 , replace the absolute values of y with the usual ones, and remove the function $\text{sign}(y)$. Multiplying both sides of Equation (36) by $\psi_n(y)$, integrating the result from -1 to 1 in y and reducing the number of the equations to a finite value N , we arrive at the following algebraic problem

$$\sum_{n=1}^N a_n \left\{ \beta D_n \delta_{nm} + \kappa^4 \beta K_{nm} + 2\kappa^2 \beta S_{nm} - \delta \gamma \delta_{nm} + M_{nm}^{(1)} - \gamma M_{nm}^{(2)} \right\} = 0, \tag{37}$$

where

$$\begin{aligned} D_n &= \theta_n^4 - \mu \kappa^2 6\alpha_1^2, & K_{nm} &= \int_{-1}^1 (1 + \alpha_1|y|)^3 \psi_n \psi_m dy, & S_{nm} &= \int_{-1}^1 (1 + \alpha_1|y|)^3 \psi_n' \psi_m' dy, \\ M_{nm}^{(1)} &= \int_{-1}^1 \psi_n \psi_m dy, & M_{nm}^{(2)} &= \int_{-1}^1 \Phi_n(y, 0) \psi_m dy. \end{aligned}$$

The resulting system of linear equations for the principal coordinates a_n in the series (18) can be written in matrix form

$$\left\{ \beta \left[D + \kappa^4 K + 2\kappa^2 S \right] + M_1 - \gamma [\delta I + M_2] \right\} a = 0, \tag{38}$$

where all matrices $D = \text{diag}\{D_n\}$, $K = \{K_{nm}\}$, $S = \{S_{nm}\}$, $M_1 = \{M_{nm}^{(1)}\}$, $M_2 = \{M_{nm}^{(2)}\}$ are symmetrical, I —identity matrix. Nontrivial solution of the resulting system of equations exist if the determinant of the matrix in curly brackets is equal to 0. Considering this condition, frequencies ω are calculated for each κ . In general, there will be infinitely

many such relations, $\omega_n(\kappa)$. In the reduced case, we calculate only first N frequencies. The accuracy of the calculations increases with the number N . Dispersion relations are numbered being the smallest for $n = 1$ and increasing with the number n for the same κ in both cases. Each dispersion relation corresponds to the mode of ice oscillations in the channel with unique profile $F_n(y)$ across the channel.

4. Numerical Results and Discussion

Calculations of periodic hydroelastic waves and their characteristics were carried out for parameters of the problem corresponding to the experimental ice tank at the Sholem Aleichem Amur State University in Birobidzhan (see [31]): $H = 1$ m, $2b = 3$ m, ice thickness in the tank is chosen to be equal to 0.0035 m. The parameters of ice and liquid in the calculations were: $\rho_i = 917$ kg/m³, $\rho_\ell = 1024$ kg/m³, $\mu = 0.3$, $E = 4.2 \times 10^9$ Pa. The units of all presented values of h_0 , h_* and h_1 are meter. The amplitude of the hydroelastic waves A can be arbitrary. Minimum and maximum values of the ice thickness change in the calculations. Typical values of the thickness and the corresponding values of the parameters α describing the change in the thickness, which were used in our calculations, are listed in Table 1. The average thickness h_* in all calculations did not change and is equal to 0.0035 m unless otherwise mentioned. Inclination angles of the plate surface are denoted by η_1 and η_2 in Case 1 and in Case 2, respectively. For the considered parameters of the problem in the presented calculations, the inclination angle never exceeds 0.002 rad. As it was formulated in Section 2, the linearized kinematic condition at the ice/liquid interface including inclination of the plate is

$$w_t = 0.5h'_i(y)\varphi_y + \varphi_z.$$

The derivative $h'_i(y)$ is equal to $\tan(\eta_{1,2})$ depending on the case. For the considered parameters of the problem, $\eta_{1,2} \ll 1$ and $\tan(\eta_{1,2})$ is of order $\eta_{1,2}$. Therefore, the term with $h'_i(y)$ is negligible in the kinematic condition.

Table 1. Parameters of the thickness used in the study.

h_0 (m)	h_1 (m)	h_0/h_*	α_1	α_2	η_1 (rad)	η_2 (rad)
0.00345	0.00355	0.98	0.0028	0.014	0.00003	0.000016
0.0025	0.0045	0.7	0.8	0.28	0.00067	0.00033
0.0015	0.0055	0.43	2.7	0.57	0.001	0.00067
0.0005	0.0065	0.14	12	0.86	0.002	0.001

The algorithm of calculations has a few steps: first, the values of η_n are calculated from the boundary conditions (20) in Cases 1 and 2, then, the functions ψ_n are determined in each case and the dispersion relations $\omega_n(k)$ are calculated as values for which the determinant of the matrix in (38) is equal to 0. Hydroelastic waves with wavelengths $\lambda > 0.63$ m are considered. It means $0 < k < 10$ m⁻¹. Frequencies $\omega_n(k)$ are determined for each value of k from this interval with a given step Δk . The calculations were carried out for waves with the frequencies from the interval $0 < \omega < 100$ s⁻¹. For each k from the indicated interval of wavenumbers, the frequency interval was divided into subintervals of length 1 and the determinant was calculated at the boundary points. We chose the subintervals on which the determinant changes its sign, and the roots of the equation $det(R) = 0$, where R is the matrix in Equation (38), were calculated by the bisection method with an accuracy 10^{-12} . The number of the modes N in the series (18) was varied from 5 to 50 to validate the convergence of the results. The first dispersion curves coincide with visual accuracy already starting from $N = 5$. In general, for most of the presented results, $N = 10$ –15. The profiles of the hydroelastic modes $F_n(y)$ are calculated by Equation (18) with the coefficients a_n calculated as eigenvectors of the matrix Equation (38), and normalized so that $max|F_n(y)| = 1$. Some of the calculations will be compared with the corresponding parameters for an ice plate with constant thickness, calculated by the method from [5].

Normalized profiles F_n of the hydroelastic modes for different values of h_0 and with $k = 3 \text{ m}^{-1}$ are shown in Figure 2. The blue lines on the left show the results for Case 1, the red lines on the right show the results for Case 2. Black lines show the results for the plate with constant thickness h_* (note that these line are covered by the solid colored lines for $h_0 = 0.00345 \text{ m}$). The parameter h_0 increases from a small value up to the value of h_* and is shown on the legend. For $h_0 = h_*$, the ice plate is of constant thickness. Corresponding values α are listed in Table 1. In Case 1, an increase of the change in ice thickness leads to narrowing of visible oscillations of the ice and increasing in the curvature of the ice deflections near the center line of the channel, where the ice has the smallest thickness. In the even case, when several local extrema exist, the maximum deflections will always be at the center of the channel. While h_0 is decreasing, the local extrema of the ice deflections shift towards the center of the channel in Case 1. In Case 2, an increase of the change in ice thickness leads to a shift of the point of maximum deflections to the left edge of the ice plate, where ice becomes thinner. In the same place of the plate, the curvature of the deflections increases. On the opposite wall, the ice deflections become smaller. In the case of several local extrema, the maximum deflections will also be in a place on the plate with the smallest ice thickness.

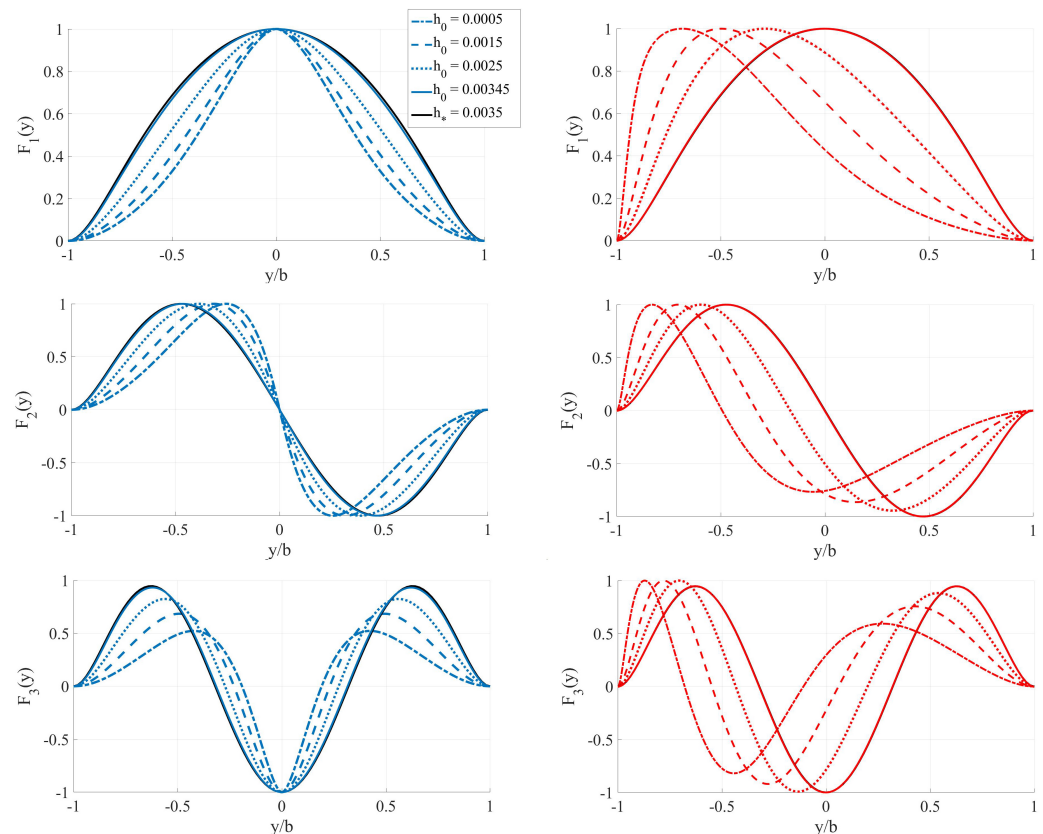


Figure 2. Profiles $F_n(y)$ of the first three hydroelastic modes across the channel for different values of h_0 and $k = 3 \text{ m}^{-1}$. Blue lines (left column)—Case 1, red lines (right column)—Case 2. Black lines show the results for the plate with constant thickness h_* (note that these line are covered by the solid colored lines for $h_0 = 0.00345 \text{ m}$).

Dispersion relations for the first four hydroelastic modes in both cases are shown in Figure 3. Blue lines show results for Case 1, red lines show the results for Case 2, black—results for the plate with constant thickness equal to h_* . The dispersion relations for the non-uniform plate are shown for two different values of h_0 , $h_0 = 0.0025 \text{ m}$ and $h_0 = 0.0005 \text{ m}$. It is seen that for $h_0 = 0.0025 \text{ m}$, all three lines are almost indistinguishable if $k < 3 \text{ m}^{-1}$. In general, within the considered intervals of wavenumbers and frequencies, the dispersion relations in Case 1 and in Case 2 are close to each other but can be rather

different from the same parameters of a plate with constant thickness. When k is near to 0, the dispersion relations in Case 1 are slightly larger than ones in Case 2, but with a further increase in the wavenumber, the dispersion relations in Case 2 increase faster and become larger. The change of h_0 has the same effect on the dispersion relations in both cases. The change in ice thickness increases rapidly when we decrease the minimum value h_0 and correspondingly increase the maximum value h_1 of the ice thickness. This change leads to a decrease in the wave frequencies for fixed wavenumbers. The lower modes are more subjected to this change. For example, for $h_0/h_* \approx 0.7$, the dispersion relations of the third and fourth modes are visually identical with ones for a plate with constant thickness equal to h_* , see Figure 3a.

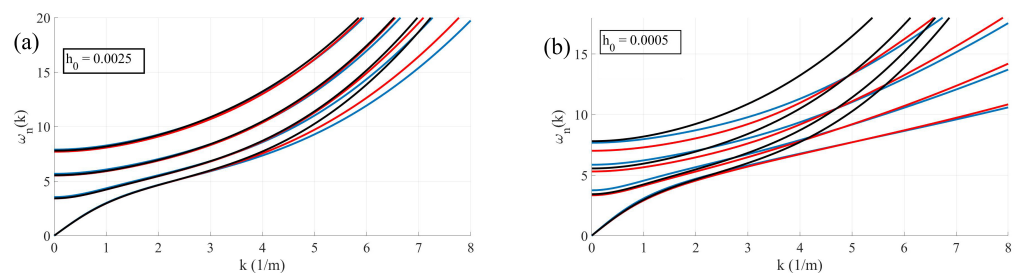


Figure 3. Dispersion relations for the first four hydroelastic modes. Black lines show results for the ice with constant thickness $h_* = 0.0035$ m, blue lines—Case 1, red lines—Case 2. (a)— $h_0 = 0.0025$ m, (b)— $h_0 = 0.0005$ m.

The effect of the change in ice thickness on the characteristics of hydroelastic waves is shown in detail in Figure 4. This figure shows dispersion relations (a), phase (b) and group (c) speeds for the first two modes in both cases. Blue lines correspond to Case 1, red lines correspond to Case 2, black line corresponds to the results for a plate with constant thickness h_* . Parameters of the ice thickness are listed in the Table 1 and on the legend of the first picture. For the considered parameters, the results of calculations for the plate with non-uniform thickness visually coincide with the results for the plate with constant thickness when $h_0 = 0.00345$ m, i.e., $h_0/h_* \approx 0.98$. The dispersion relations, phase and group speeds decrease as the change in ice thickness and parameter α increase. In general, values of these waves parameters in Case 1, as noted in the previous section, are always less than same values in Case 2, with the exception of a small interval of wavenumbers near 0. Note that the phase and group speeds of the first mode when $k \rightarrow 0$ approach the values of the same parameters for a plate with constant thickness from above in Case 1, and from below in Case 2. The minimum phase speed of each mode changes insignificantly, but the wavenumbers corresponding to the minimum of these speeds increase significantly. For example, in the case $h_0 = 0.0005$ m, the wavenumber for the minimum speed of the first mode is greater than 10 (Figure 4b). In contrast to a plate with constant thickness, for the plate with non-uniform ice thickness and for the same speeds of the waves, shorter hydroelastic waves in the channel will propagate. In addition, as the change in thickness increases, the waves will become even shorter.

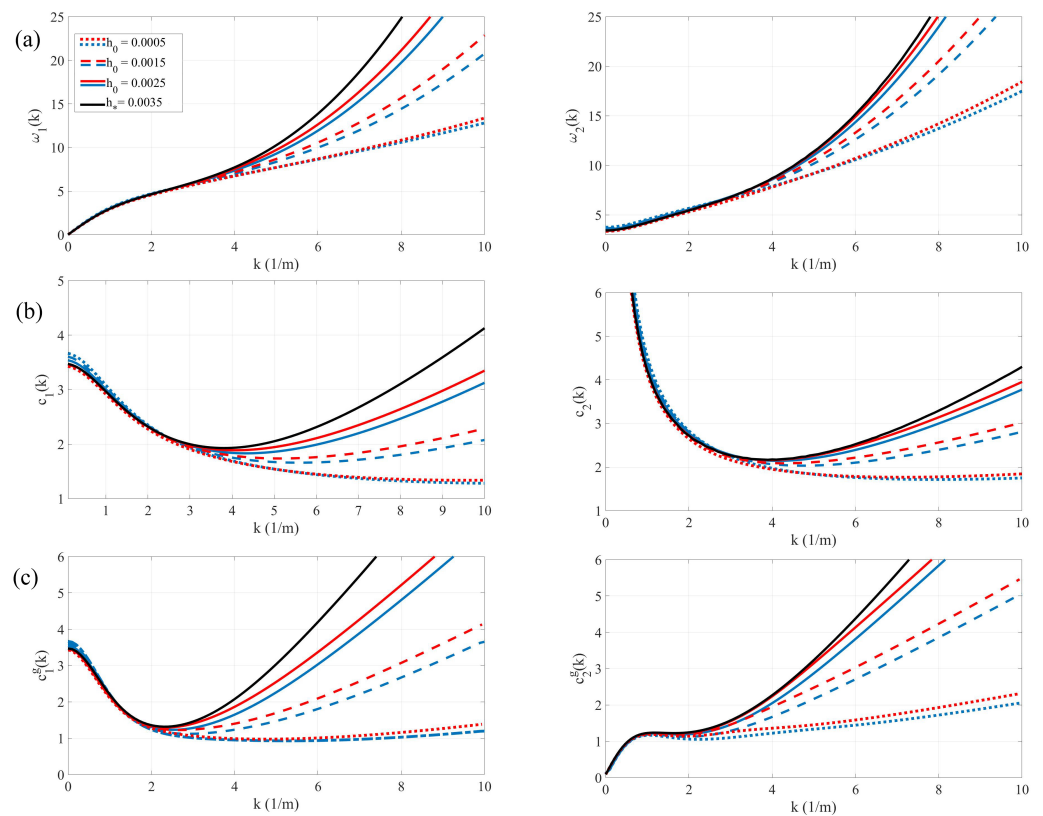


Figure 4. Dispersion relations (a), phase (b) and group (c) speeds of the first (left) and second (right) modes for different values of h_0 . Red lines show the results for Case 1, blue—for Case 2. The black line shows the results for the plate with constant thickness equal to $h_* = 0.0035$ m.

One may think that the characteristics of hydroelastic waves for the plate with non-uniform thickness are closest to the characteristics of a plate with constant thickness equal to the average value h_* . Dispersion relations and phase speeds for the first and third modes in comparison with the results for a plate with constant thickness equal to h_0 , h_* and h_1 are shown in Figures 5 and 6. The dispersion relations are shown in Figure 5. The phase speeds are shown in Figure 6. The results presented in these figure on the left side are for $h_0 = 0.0025$ m for a plate with a linear thickness and for three cases of a constant thickness plate $h_i = h_0 = 0.0025$ m, $h_i = h_* = 0.0035$ m and $h_i = h_1 = 0.0045$ m (thinner, middle and thicker thickness values for the linear plate considered). The results presented in these figure on the right side are for $h_0 = 0.0015$ m for a plate with a linear thickness and the corresponding three cases of a constant thickness plate. For modes with a large index, the characteristics of hydroelastic waves actually behave as in the case of a plate with constant thickness equal to average value h_* . This can be also correct for cases with a large change in the ice thickness, compare the results between non-uniform plate and plate with constant thickness (blue and red lines with black line in Figures 5 and 6b on the right side). These conclusions are incorrect for lower modes. For these modes, the wave characteristics can be a little closer to the values of characteristics for the ice plate with constant thickness equal to h_0 (blue and red lines in comparison with the green line in Figures 5 and 6a on the left).

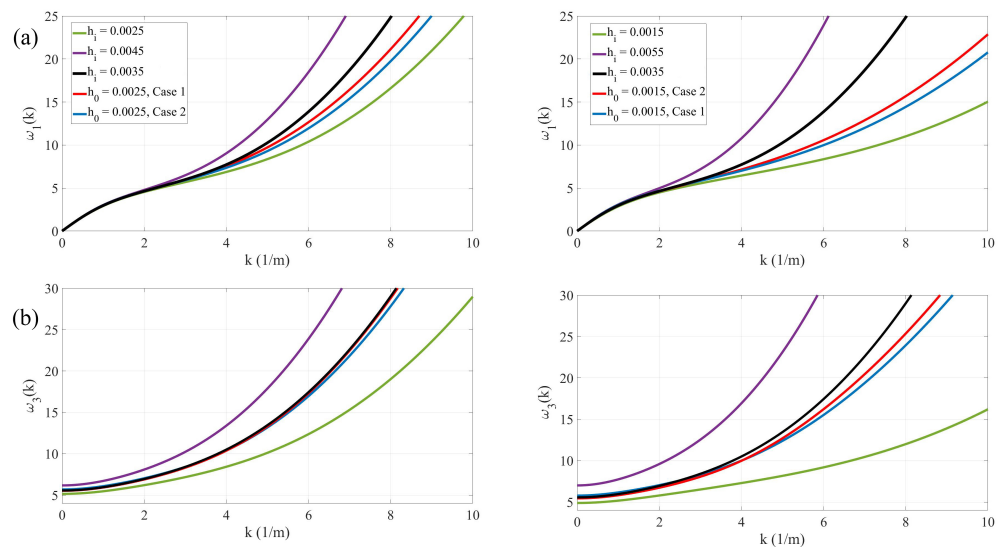


Figure 5. Dispersion relations of the first (a) and third (b) modes for $h_0 = 0.0025$ m (left) and for $h_0 = 0.0015$ m (right) for non-uniform plate and for uniform plate with h_i equal to values of h_0 , h_* and h_1 of the ice thickness of non-uniform plate (these values are shown in the legend). Red lines show the results for Case 1, blue—for Case 2. Black line shows the results for a plate with constant thickness equal to $h_* = 0.0035$ m. Purple and green lines show the results for a plate with constant thickness equal to h_1 and h_0 , respectively.

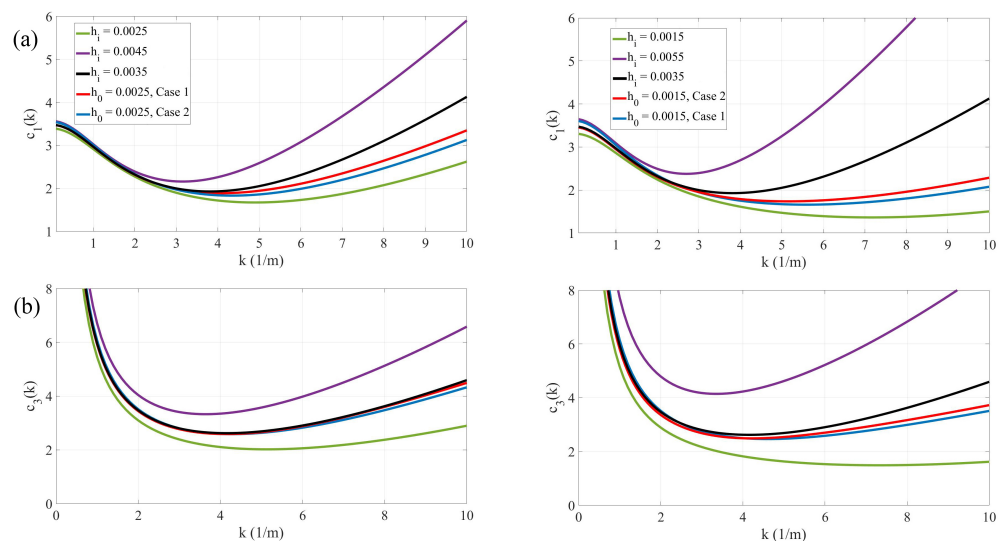


Figure 6. Phase speeds of the first (a) and third (b) modes for $h_0 = 0.0025$ m (left) and for $h_0 = 0.0015$ m (right) for non-uniform plate and for uniform plate with h_i equal to values of h_0 , h_* and h_1 of the ice thickness of the non-uniform plate. Colors of lines correspond to the same in Figure 5.

One of the practical points of interest are so-called critical speeds. At this speed, ice plate deflections are limited only by dissipation and nonlinearities. The critical speeds of the hydroelastic waves in a frozen channel help understand and predict the response of the ice cover to a moving load depending on its speed (see [10]). Squire [3] wrote about the critical speed of hydroelastic waves: phase speed c has a minimum, denoted by c_{min} , above which flexural-gravity waves can propagate freely and below which no such waves are generated. The minimum is associated with the critical speed v_{crit} at which deflection of the floating ice plate is greatest when a load travels by. The corresponding method of icebreaking was studied theoretically, numerically and experimentally [28–31] by Kozin and his group. In this method, called the “resonant method of ice-breaking”, an air-cushion

vehicle moves at a speed close to the critical speed of hydroelastic waves on the ice sheet. It was observed [7] that flexural waves, which are caused by a vehicle moving across a thin elastic plate, occur if the speed of the vehicle exceeds the minimum c_{min} of the phase speed of elastic-gravity free waves in the plate. The plate response is approximately quasi-static for lower speeds of the vehicle. It was concluded in [7] that the amplified response at the critical speed $V = c_{min}$ corresponds to an accumulation of energy underneath the source, since c_{min} coincides with the group speed. The speed $c(0)$ has a similar effect on the ice deflections and can be considered critical too. For the one-dimensional model of ice cover in a channel [43] and the ice plate of infinite extent [3], there is only one dispersion relation between frequency and the length of hydroelastic wave and, correspondingly, one value c_{min} , one value $c(0)$ and, therefore, two critical speeds. For a channel covered with ice, there are infinitely many dispersion relations and corresponding critical speeds.

The critical speeds U_n^{crit} of the first four modes and the corresponding wavenumbers as functions of the parameter h_0/h_* are shown in Figure 7. The more the thickness of ice plate changes, the lower the critical speeds are. When h_0/h_* tends to 1, the critical speeds approach the asymptote and the critical speeds for a plate with constant thickness h_* . Wavenumbers for critical speeds increase significantly when $h_0/h_* \rightarrow 0$. For example, if $h_0 = 0.0005$ m the values of the critical speeds and corresponding wavenumbers are: $U_1^{crit} = 0.77$ m/s, $k_1^{crit} = 31.92$ m⁻¹, $U_2^{crit} = 1.15$ m/s, $k_2^{crit} = 23.38$ m⁻¹, $U_3^{crit} = 1.6$ m/s, $k_3^{crit} = 15.85$ m⁻¹, $U_4^{crit} = 2.07$ m/s, $k_4^{crit} = 12.7$ m⁻¹. Note that the number of the mode with the shortest wavelength of the critical speed changes in inverse proportion to h_0/h_* . For a large change in the thickness (small h_0/h_*), critical speeds for modes with a large index have greater wavelength; when $h_0/h_* \rightarrow 0$, the values of the wavenumbers of critical speeds are ordered in ascending order according to the mode number. Accordingly, it can be expected that when an external load moves along an ice cover with non-uniform thickness, starting its movement from a state of rest and progressively increases its speed, firstly, short waves will be generated in the ice. The finite value $c_1(0)$ of the phase speed when $k \rightarrow 0$ exists only for the first mode. In the considered case for the plate with constant thickness $h_* = 0.0035$ m, this speed is $c_1(0) = 3.47$ m/s. This speed is weakly affected by the non-uniform thickness of ice and the corresponding change of h_0 (see Figure 6a). For example, for the plate within Case 2, with $h_0 = 0.0015$ m, $c_1(0) = 3.58$ m/s, which means the difference in these speeds is about 3% between plates with constant and non-uniform thickness. Note that in all cases, the critical speeds of the first four modes are less than $c_1(0)$ for the considered channel.

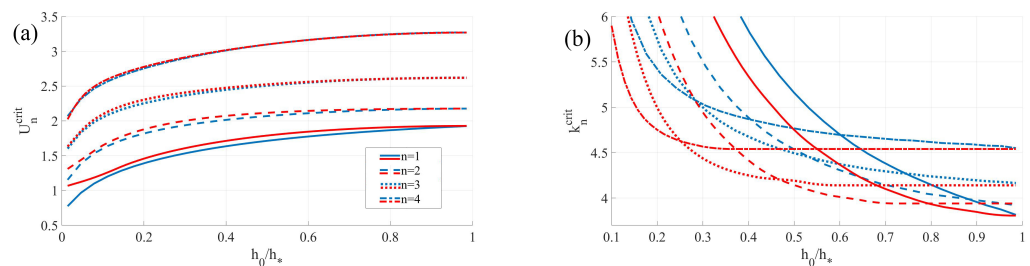


Figure 7. The critical speeds of the first four modes as a function of the parameter h_0/h_* (a). Corresponding wave numbers of critical speeds (b).

Distribution of Strains in the Ice Cover

Deformations in the ice cover are described within the linear theory under the assumption that the values of $w_x^2 + w_y^2$ are small and stresses in the plate are proportional to strains. Note that ice is a rather brittle material; therefore, limiting stresses in the ice plate, leading to its breaking, are reached earlier than the strains of the plate and go beyond the linear theory.

Since the solution to the problem is sought in the form of waves traveling along the channel, it is a function of a phase $\theta(x, t) = \kappa x + t$ and has the form

$$w(x, y, t) = F(y) \cos(\theta).$$

The absolute maximum strain in a hydroelastic wave is a function of the dimensionless parameters $\alpha, \beta, \gamma, \delta, \kappa, h$ and is calculated by the formula

$$\varepsilon_{ABS} = \max_{-1 \leq y \leq 1} [\varepsilon_{\max}(y)], \tag{39}$$

where

$$\varepsilon_{\max} = \max_{0 \leq \theta \leq 2\pi} \varepsilon(y, \theta). \tag{40}$$

The magnitude $h_0 A / 2b^2$ is chosen as the scale of the strains in Case 1, and $h_* A / 2b^2$ in Case 2.

The strain field in the ice plate is described by the strain tensor [44]

$$T_\varepsilon = -\zeta \begin{bmatrix} w_{xx} & w_{xy} \\ w_{xy} & w_{yy} \end{bmatrix},$$

where ζ is a dimensionless variable varying over the thickness of the plate, $-(1 + \alpha_1|y|) \leq \zeta \leq (1 + \alpha_1|y|)$ in Case 1, $-(1 + \alpha_2y) \leq \zeta \leq (1 + \alpha_2y)$ in Case 2.

To estimate the maximum strain at a point (x, y) of the ice cover at time t , it is necessary to determine the principal strains and find their maximum. Within the linear theory, the maximum stresses and strains are achieved on the plate surface, at $|\zeta| = 1 + \alpha_1|y|$ in Case 1 and $|\zeta| = 1 + \alpha_2y$ in Case 2. The principal strains ε are determined through the eigenvalues of the tensor T_ε by the formula

$$\varepsilon^{(1,2)}(y, \theta) = \frac{\zeta}{2} [-a \cos(\theta) \pm \sqrt{(b^2 - c^2) \cos^2(\theta) + c^2}], \tag{41}$$

where the notation is introduced

$$a(y) = F''(y) - \kappa^2 F(y), \quad b(y) = F''(y) + \kappa^2 F(y), \quad c(y) = 2\kappa F'(y).$$

The functions (41) are smooth with respect to the variable θ ; therefore, the maximum (40) is achieved at the extremal point from the condition

$$\frac{d\varepsilon}{d\theta} = \frac{\zeta}{2} \left[a \mp \frac{(b^2 - c^2) \cos(\theta)}{\sqrt{(b^2 - c^2) \cos^2(\theta) + c^2}} \right] \sin(\theta) = 0. \tag{42}$$

The solution of Equation (42) determines the maximum principal strains along the phase in the form

$$\varepsilon_{\max}^{(1)} = \frac{1 + \alpha y}{2} (|a| + |b|), \quad \varepsilon_{\max}^{(2)} = \frac{1 + \alpha y}{2} |c| \sqrt{\frac{b^2 - c^2 - a^2}{b^2 - c^2}}.$$

It is easy to show that ε_{\max} has the form

$$\varepsilon_{\max} = \begin{cases} \varepsilon_{\max}^{(1)}, & c^2 - b^2 \leq |ab|; \\ \varepsilon_{\max}^{(2)}, & c^2 - b^2 > |ab|. \end{cases}$$

Note that, in fact,

$$\varepsilon_{\max}^{(1)} = (1 + \alpha y) \max\{|F''|, \kappa^2|F|\},$$

that means the absolute maximum strain corresponds to the maximum transverse $|w_{yy}|$ (possible cracks along the channel) or longitudinal $|w_{xx}|$ (possible cracks across the channel) strains relative to the channel axis. The value $\varepsilon_{\max}^{(2)}$ corresponds to the maximum

strains, which are neither longitudinal nor transverse, forming a nonzero angle with the channel axis.

The maximum scaled strains along the phase for the first three modes in both cases for different values of k and for $h_0 = 0.0025$ m are shown in Figure 8 as functions of y . Results for Case 1 are shown on the left, for Case 2 on the right of the figure. The scale of the strains is $A/(2b^2)$. In Case 1 for small k , the maximum strains are achieved at the channel walls and correspond to longitudinal strains. This shows that the possible detachment of the ice cover will be from both walls of the channel, at the same time. Further, with the increase in k , the strains at the channel walls decrease and strains inside the plate increase. The maximum strains inside the plate are close to the midpoint but not at it directly. It can be seen that in Case 2, at small k , the absolute maximum of strains correspond to longitudinal strains too and, for all hydroelastic modes, is achieved at the thinner (left) edge of the plate $y = 1$. This shows that the possible detachment of the ice cover will be from the left bank. With the increase in k , longitudinal strains (dotted lines) inside the channel grow faster than the transverse ones, and at a certain value of k , these strains become absolute maximum and remain so with the further increase in k in both cases. This effect is observed for all values of α considered in the calculations. At first, it appears only for the first hydroelastic mode of the plate, then, with the increase in k , it also appears in the second mode and then appears for all hydroelastic modes. It is interesting to note that, in Case 2, for the higher modes, the internal maximum with increasing k shifts towards thicker edge. In Case 1, with the increase in the mode number, the maximum strains can shift away from the central line of the channel closer to the midpoints of the half-intervals to the left and right of the center of the channel. Note that the combined strains for all considered values of α never become absolute maximum.

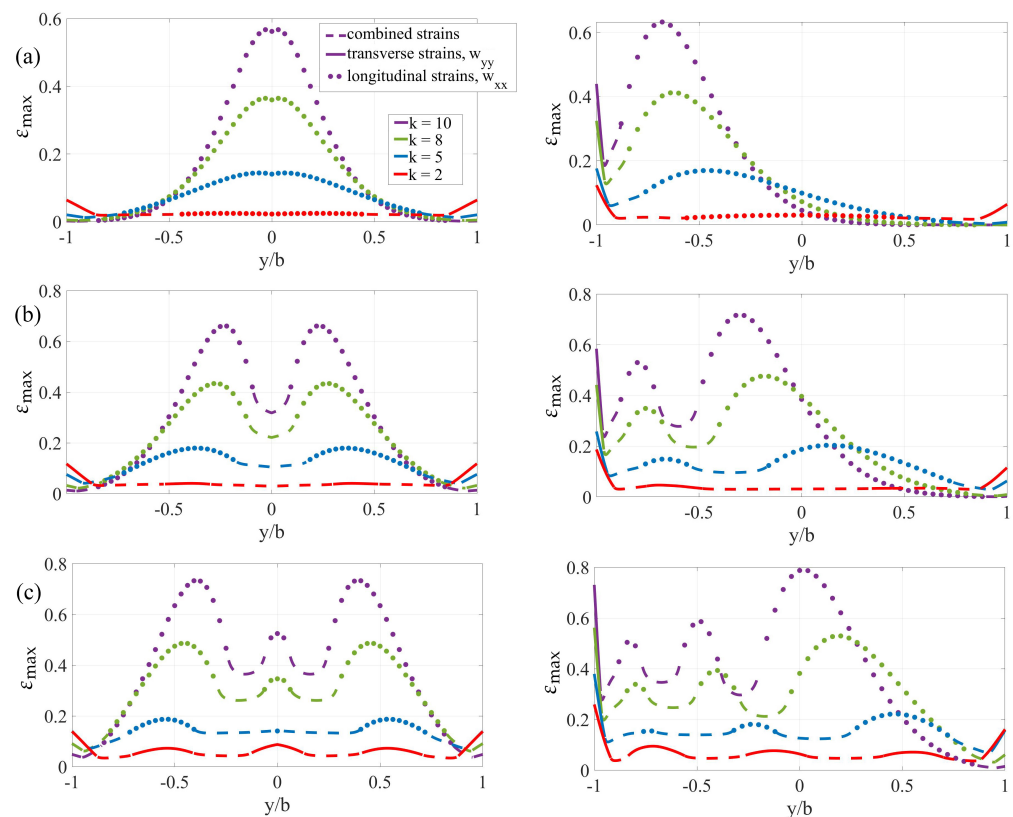


Figure 8. The scaled maximum strains $\epsilon_{max}(y)$ in the hydroelastic wave along the phase for the first three modes for different values of k (see legend) and with $h_0 = 0.0025$ m. The results for Case 1 are shown on the left of the figure, for Case 2—on the right. The longitudinal strains are shown by dotted line (markers), transverse strains—by the solid line, combined strains—by the dashed line. The scale is $A/(2b^2)$. Here, (a)—first mode, (b)—second and (c)—third one.

The same results as in Figure 8, but for $h_0 = 0.0015$ m, are shown in Figure 9. It is interesting to note that for this minimum thickness of non-uniform ice, the maximum strains remain the transverse ones at the thin edge of ice plate in Case 2. In Case 1 for the third mode, the maximum strains at the center of the channel can be both transverse ($k = 5 \text{ m}^{-1}$) or longitudinal $k = 8, 10 \text{ m}^{-1}$. In Case 2, the absolute value of maximum strains is 1.5 times higher than in Case 1. If one compares Figures 8 and 9, it can be seen that the strains have been increased for Case 2, but have been decreased for Case 1. Therefore, the change in ice thickness has an important role in determining the absolute maximum strains.

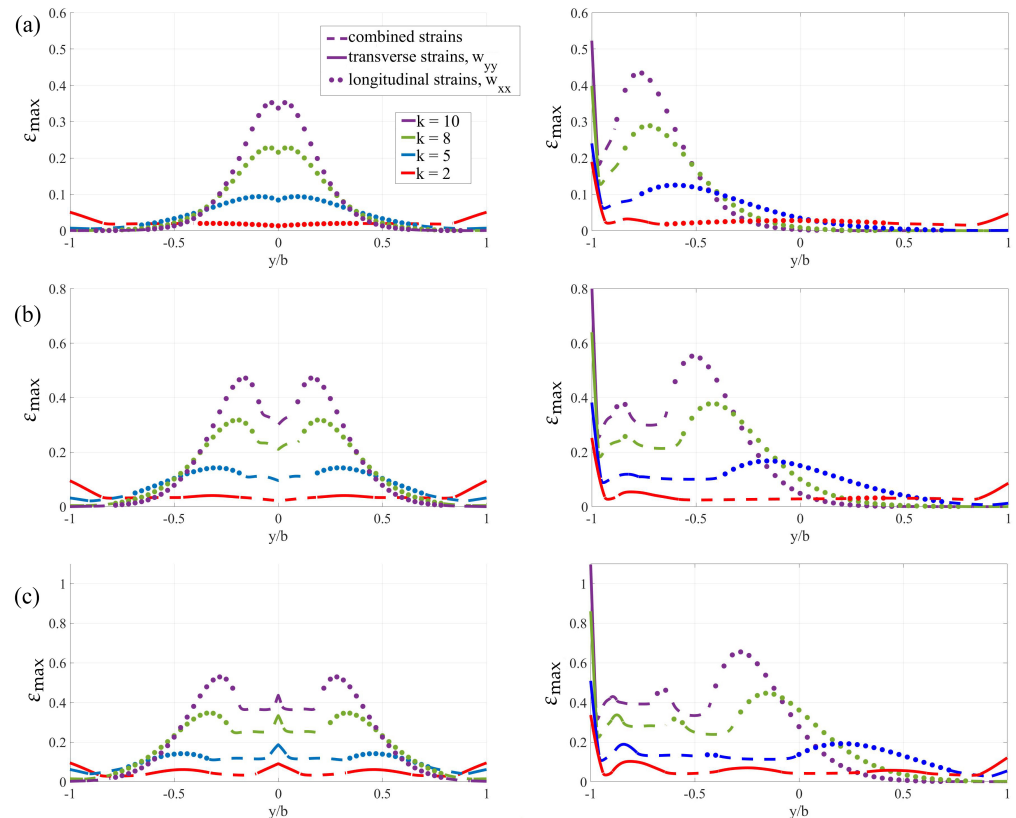


Figure 9. The scaled maximum strains $\epsilon_{max}(y)$ in the hydroelastic wave along the phase for the first three modes for different values of k and with $h_0 = 0.0015$ m. Here, (a)—first mode, (b)—second and (c)—third one. All notations are the same as in Figure 8.

Scaled absolute maximum strains $\epsilon_{ABS} = \max_{-1 \leq y \leq 1} (\epsilon_{max}(y))$ are shown in Figure 10 as functions of wavenumber k for 4 different values of h_0 (see legend). For lower modes, the behavior of strains is generally the same depending on k . First, the absolute strains correspond to transverse ones near the walls (or the left wall in Case 2), and with an increase in k , these strains decrease. Further, the absolute strains are replaced by longitudinal ones inside the plate, which grow with an increase in k . For modes with a number 3 or more, strains always grow with an increase in k , starting from $k = 0$. Note that for these modes, for the considered interval of wavenumbers and for some values of h_0 , there are no changes in directions of the absolute strains. The behavior of absolute strains depending on h_0 differs significantly for the considered cases. In Case 2, a decrease in h_0 (an increase in the change in ice thickness) leads to an increase in the absolute strains, in particular, to an increase in the strains at the left wall, where ice becomes thinner. This is due to a large increase in the curvature of ice oscillations near this wall. In Case 1, an increase in the change in ice thickness leads to a decrease in absolute strains. For long waves, the maximum strains are achieved at the edges of the plate and decrease with increasing thickness of the edge.

For shorter waves, the maximum strains correspond to strains inside the plate. However, these strains, usually located near the midpoint, do not grow fast enough. Their growth depends on h_0 in a non-obvious way. For example, for the third mode (see Figure 10c), for $h_0 = 0.0005$ m (strong change in thickness), the absolute strains do not change their directions and, for different k , can be either more or less than the strains for $h_0 = 0.0015$ m (blue and red lines in the figure). For $k \approx 5.4 \text{ m}^{-1}$ for the same mode, the absolute strains in the considered range of h_0 differ from each other by no more than 10 percent. In Case 2, for the same mode and the same k , the absolute strains for $h_0 = 0.0005$ m are 3 times higher than those for $h_0 = 0.0034$ m (purple and red lines for $k \approx 5.4 \text{ m}^{-1}$ in Figure 10c on the right). This emphasizes the importance of the distribution of non-uniform ice thickness across a channel, especially when seeking places of possible ice breaking.

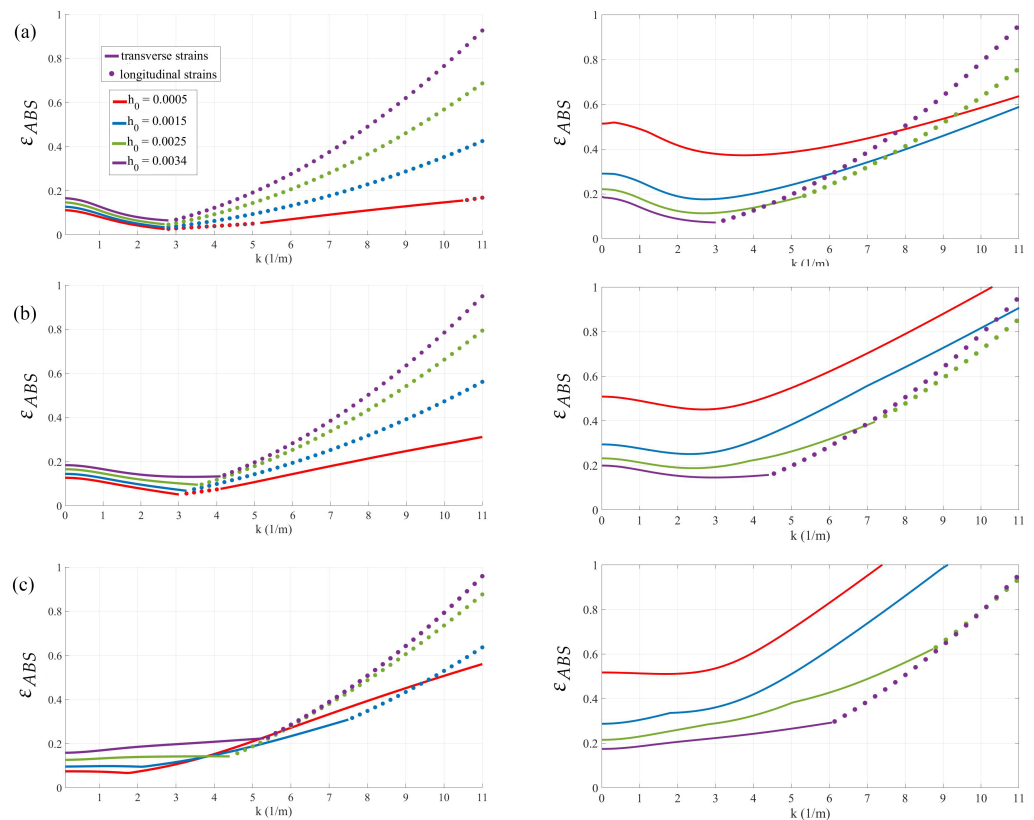


Figure 10. The scaled absolute maximum strains, $\epsilon_{ABS} = \max \epsilon_{max}(y)$ for the first three modes as functions of k for 4 different values of h_0 (see legend). Here, (a)—first mode, (b)—second and (c)—third one. The results for Case 1 are shown on the left of the figure, for Case 2, on the right. The longitudinal strains are shown by the dotted line (markers), transverse strains—by the solid line. The scale is $A/(2b^2)$.

5. Conclusions

The linear problem of hydroelastic waves propagating along a channel with an ice cover frozen to the walls of the channel was investigated for two cases of linear changes in ice thickness. Case 1 is for symmetric ice thickness, and Case 2—for thin ice on one bank of the channel and thick ice on the other bank (asymmetric case). Both problems were solved by the normal mode method. The normal modes were presented analytically, which make the general solution more accurate. The normal mode method allows us to reduce the problem for periodic waves along the channel to a system of linear equations for the coefficients of deflection expansion by modes. These systems are similar for both cases, but the matrices in them are different for each of these cases. The resulting systems were solved numerically by the reduction method.

The shapes of ice plate oscillations, dispersion curves, phase, group and critical speeds of the waves were obtained. All results were compared between the Cases 1 and 2 and with the case of constant ice thickness for the different ratio between minimum h_0 and average h_* values of ice thickness. It was shown that all hydroelastic wave parameters tend to corresponding ones for homogeneous ice thickness h_* with $h_0/h_* \rightarrow 1$.

As in the case of constant thickness ice in the channel [5,26], there is infinite number of hydroelastic waves with the same length and different form across the channel propagating along the channel. These waveforms have been obtained and it was shown that the maximum deflection of the ice are displaced toward the thinner part of the plate as the ratio h_0/h_* decreases (in Case 2 and for the odd waveforms in Case 1). It was shown that for long waves ($k < 3$), the dispersion curves, and consequently the phase and group velocities, are almost indistinguishable from the corresponding curves for a plate with constant thickness h_* . As k increases, the frequencies $\omega_n(k)$ decrease for both cases under consideration compared to the case of ice of constant thickness. This deviation is most clearly seen for the first modes of plate vibrations. Note that the frequency $\omega_n(k)$ decreases as the thickness of the plate. That is, for a plate with a linearly varying thickness, the dispersion curves, as the ratio h_0/h_* decreases, show that the oscillations behave in a manner closer to those in the thinner homogeneous plate.

The investigation showed that for the plates under consideration, the critical speeds are lower than for a plate with constant thickness h_* for all forms of propagating waves. The greatest difference appears at $h_0/h_* \rightarrow 0$. The critical velocities for the symmetric case are slightly lower than for the asymmetric case. In addition, the wavenumbers k which correspond to them essentially depend both on the ratio h_0/h_* and on Case 1 or 2.

The strain distributions in the propagating hydroelastic waves were analyzed. It was concluded that strains are maximum at the bank of channel for long waves and move inside of the channel for short waves. In case 1, the maximum stretch is achieved inside the plate—close to the center, but not in the midpoint. For the asymmetric case, it was shown that for long waves, the most probable plate failure corresponds to transverse strains at the thinnest edge of the plate, which can lead to breakaway of the ice from the corresponding bank. This character of variations in the distribution of strain across the channel is a feature of the hydroelastic behavior of an ice plate with non-uniform thickness of the ice cover.

The results of the study show that not only the average and the smallest values of the thickness of non-uniform ice are important, but also the specific distribution of the ice thickness across the channel. This is indicated by the difference in dispersion relations and other hydrodynamic characteristics in symmetric and asymmetric cases.

Author Contributions: Conceptualization, T.K., K.S. and E.B.; methodology, T.K., K.S. and E.B.; software, K.S. and E.B.; validation, K.S., E.B. and K.Z.; formal analysis, T.K., K.S., E.B. and K.Z.; investigation, K.S., E.B. and K.Z.; resources, K.S., E.B. and K.Z.; writing—original draft preparation, K.S. and K.Z.; writing—review and editing, K.S. and T.K.; and visualization, K.Z. and E.B. All authors have read and agreed to the published version of the manuscript.

Funding: The study was funded by RFBR and TUBITAK according to the research project—20-58-46009 Loads on engineering structures in sea ice.

Institutional Review Board Statement: Not applicable.

Informed Consent Statement: Not applicable.

Data Availability Statement: Data of numerical calculations are available upon request.

Conflicts of Interest: The authors declare no conflict of interest.

References

1. Greenhill, A.G. Wave motion in hydrodynamics. *Am. J. Math.* **1886**, *9*, 62–96. [[CrossRef](#)]
2. Kheysin, Y. Moving load on an elastic plate which floats on the surface of an ideal fluid. *Izv. Akad. Nauk SSSR Otd. Tekh. Nauk Mekh. Mashinostr.* **1963**, *1*, 178–180. (In Russian)
3. Squire, V.A.; Hosking, R.; Kerr, A.; Langhorne, P.J. *Moving Loads on Ice Plates*; Kluwer: Dordrecht, The Netherlands, 1996.

4. Squire, V.A. Ocean wave interactions with sea ice: A reappraisal. *Ann. Rev. Fluid Mech.* **2020**, *52*, 37–60. [[CrossRef](#)]
5. Korobkin, A.A.; Khabakhpasheva, T.I.; Papin, A.A. Waves propagating along a channel with ice cover. *Eur. J. Mech.-B/Fluids* **2014**, *47*, 166–175. [[CrossRef](#)]
6. Ren, K.; Wu, G.X.; Li, Z.F. Hydroelastic waves propagating in an ice-covered channel. *J. Fluid Mech.* **2020**, *886*, A18. [[CrossRef](#)]
7. Hosking, R.J.; Sneyd, A.D.; Waugh, D.W. Viscoelastic response of a floating ice plate to a steadily moving load. *J. Fluid Mech.* **1988**, *196*, 409–430. [[CrossRef](#)]
8. Wang, R.; Shen, H.H. Gravity waves propagating into an ice-covered ocean: A viscoelastic model. *J. Geophys. Res. Oceans.* **2010**, *115*. [[CrossRef](#)]
9. Chen, H.; Gilbert, R.P.; Guyenne, P. Dispersion and attenuation in a porous viscoelastic model for gravity waves on an ice-covered ocean. *Eur. J. Mech.-B/Fluids* **2019**, *78*, 88–105. [[CrossRef](#)]
10. Shishmarev, K.A.; Khabakhpasheva, T.I.; Korobkin, A.A. The response of ice cover to a load moving along a frozen channel. *Appl. Ocean Res.* **2016**, *59*, 313–326. [[CrossRef](#)]
11. Meylan, M.H.; Bennetts, L.G.; Peter, M.A. Water-wave scattering and energy dissipation by a floating porous elastic plate in three dimensions. *Wave Motion.* **2017**, *70*, 240–250. [[CrossRef](#)]
12. Zavyalova, K.N.; Shishmarev, K.A.; Korobkin, A.A. The response of a poroelastic ice plate to an external pressure. *J. Sib. Fed. Univ. Math. Phys.* **2021**, *14*, 87–97. [[CrossRef](#)]
13. Părău, E.I.; Dias, F. Nonlinear effects in the response of a floating ice plate to a moving load. *J. Fluid Mech.* **2002**, *460*, 281–305. [[CrossRef](#)]
14. Bonnefoy, F.; Meylan, M.H.; Ferrant, P. Nonlinear higher-order spectral solution for a two-dimensional moving load on ice. *J. Fluid Mech.* **2009**, *621*, 215–242. [[CrossRef](#)]
15. Plotnikov, P.I.; Toland, J.F. Modelling nonlinear hydroelastic waves. *Philos. Trans. R. Soc. Lond. A Math. Phys. Eng. Sci.* **2011**, *369*, 2942–2956. [[CrossRef](#)] [[PubMed](#)]
16. Il'ichev, A.T. Solitary wave packets beneath a compressed ice cover. *Fluid Dyn.* **2016**, *51*, 327–337. [[CrossRef](#)]
17. Il'ichev, A.T. Effective wavelength of envelope waves on the water surface beneath an ice sheet: Small amplitudes and moderate depths. *Theor. Math. Phys.* **2021**, *208*, 1182–1200. [[CrossRef](#)]
18. Stepanyants, Y.; Sturova, I. Waves on a compressed floating ice plate caused by motion of a dipole in water. *J. Fluid Mech.* **2021**, *907*, A7. [[CrossRef](#)]
19. Stepanyants, Y.; Sturova, I. Hydrodynamic Forces Exerting on an Oscillating Cylinder under Translational Motion in Water Covered by Compressed Ice. *Water* **2021**, *13*, 822. [[CrossRef](#)]
20. Semenov, Y.A. Nonlinear flexural-gravity waves due to a body submerged in the uniform stream. *Phys. Fluids* **2021**, *33*, 052115. [[CrossRef](#)]
21. Marchenko, A.; Haase, A.; Jensen, A.; Lishman, B.; Rabault, J.; Evers, K.-U.; Shortt, M.; Thiel, T. Laboratory Investigations of the Bending Rheology of Floating Saline Ice and Physical Mechanisms of Wave Damping in the HSVA Hamburg Ship Model Basin Ice Tank. *Water* **2021**, *13*, 1080. [[CrossRef](#)]
22. Tkacheva, L.A. Wave motion in an ice sheet with crack under uniformly moving Load. *Fluid Dyn.* **2019**, *54*, 14–32. [[CrossRef](#)]
23. Barman, S.C.; Das, S.; Sahoo, T.; Meylan, M.H. Scattering of flexural-gravity waves by a crack in a floating ice sheet due to mode conversion during blocking. *J. Fluid Mech.* **2021**, *916*, A11. [[CrossRef](#)]
24. Brocklehurst, P.; Korobkin, A.A.; Părău, E.I. Interaction of hydro-elastic waves with a vertical wall. *J. Eng. Math.* **2010**, *68*, 215–231. [[CrossRef](#)]
25. Tkacheva, L.A. Oscillations of a Cylinder beneath an Ice Cover in the Neighborhood of a Vertical Wall. *Fluid Dyn.* **2020**, *55*, 300–313. [[CrossRef](#)]
26. Batyaev, E.A.; Khabakhpasheva, T.I. Hydroelastic waves in a channel covered with a free ice sheet. *Fluid Dyn.* **2015**, *50*, 775–788. [[CrossRef](#)]
27. Bogorodsky, V.V.; Gavrilov, V.P.; Nedoshivin, O.A. *Ice Destruction: Methods and Technology*; Springer: Berlin/Heidelberg, Germany, 1987; 221p.
28. Zhestkaya, V.D.; Kozin, V.M. *Ice Breaking with Air-Cushion Vessels Using a Resonant Method*; Dal'nauka: Vladivostok, Russia, 2003; 160p. (In Russian)
29. Kozin, V.M. *The Resonant Method of Ice Breaking: Inventions and Experiments*; Academy of Natural Sciences: Moscow, Russia, 2007. (In Russian)
30. Zhestkaya, V.D. Numerical solution of the problem of an ice sheet under a moving load. *J. Appl. Mech. Tech. Phys.* **1999**, *40*, 770–775. [[CrossRef](#)]
31. Pogorelova, A.V.; Zemlyak, V.L.; Kozin, V.M. Moving of a submarine under an ice cover in fluid of finite depth. *J. Hydrodyn.* **2019**, *31*, 562–569. [[CrossRef](#)]
32. Hinchey, M.; Colbourne, B. Research on low and high speed hovercraft icebreaking. *Can. J. Civ. Eng.* **1995**, *22*, 32–42. [[CrossRef](#)]
33. Khabakhpasheva, T.I.; Shishmarev, K.A.; Korobkin, A.A. Large-time response of ice cover to a load moving along a frozen channel. *Appl. Ocean Res.* **2019**, *86*, 154–165. [[CrossRef](#)]
34. Shishmarev, K.A.; Khabakhpasheva, T.I.; Korobkin, A.A. Ice response to an underwater body moving in a frozen channel. *Appl. Ocean Res.* **2019**, *91*, 101877. [[CrossRef](#)]

35. Marchenko, A. Nonlinear Phenomena in Resonant Excitation of Flexural-Gravity Waves. *J. Ship Ocean Technol. Soc. Naval Arch. Korea* **2003**, *7*, 1–12.
36. Li, Q.S. Vibration analysis of flexural-shear plates with varying cross-section. *Int. J. Solids Struct.* **2000**, *37*, 1339–1360. [[CrossRef](#)]
37. Timoshenko, S.; Woinowsky-Krieger, S. *Theory of Plates and Shells*; McGraw-Hill Book Company, Inc.: New York, NY, USA; Toronto, ON, Canada; London, UK, 1959.
38. Chopra, I. Vibration of stepped thickness plates. *Int. J. Mech. Sc.* **1974**, *16*, 337–344. [[CrossRef](#)]
39. Li, Q.S.; Cao, H.; Li, G. Static and dynamic analysis of straight bars with variable cross-section. *Int. J. Comput. Struct.* **1996**, *59*, 1185–1191. [[CrossRef](#)]
40. Taha, M.H.; Abohadima, S. Mathematical model for vibrations of non-uniform flexural beams. *Eng. Mech.* **2008**, *15*, 3–11.
41. Nesterov, S.V.; Baydulov, V.G. Transverse oscillations of a cantilever rod of rectangular cross section and variable thickness. *J. Phys. Conf. Ser.* **2019**, *1301*, 012023. [[CrossRef](#)]
42. Korobkin, A.A.; Khabakhpasheva, T.I.; Malenica, S. Maximum stress of stiff elastic plate in uniform flow and due to jet impact. *Phys. Fluids* **2017**, *29*, 072105. [[CrossRef](#)]
43. Daly, S.F. Wave propagation in ice-covered channels. *J. Hydraul.* **1993**, *119*, 895–910. [[CrossRef](#)]
44. Gross, D.; Hauger, W.; Schroder, J.; Wall, W.A.; Bonet, J. *Engineering Mechanics*, 2nd ed.; Springer: Berlin/Heidelberg, Germany, 2013.